

We are IntechOpen, the world's leading publisher of Open Access books Built by scientists, for scientists

6,900

Open access books available

186,000

International authors and editors

200M

Downloads

Our authors are among the

154

Countries delivered to

TOP 1%

most cited scientists

12.2%

Contributors from top 500 universities



WEB OF SCIENCE™

Selection of our books indexed in the Book Citation Index
in Web of Science™ Core Collection (BKCI)

Interested in publishing with us?
Contact book.department@intechopen.com

Numbers displayed above are based on latest data collected.
For more information visit www.intechopen.com



Ceramics (Si- and Al-Based Oxides)-Graphene Hybrids and Advanced Applications

Mujtaba Ikram and Muhammad Umer Farooq

Abstract

This book chapter will describe the recent advancements in advanced carbon-ceramics based hybrid materials, enhanced properties and efficient applications. There are various fabrication methods, Firstly, authors will discuss a solvothermal/hot-pressing method which is employed to fabricate hybrids composed of cross-linked γ -Al₂O₃ nanorods and reduced graphene oxide (rGO) platelets. After calcination and hot-press processing, monoliths of Al₂O₃-rGO hybrids are obtained with improved physical properties. It is found that the oxygen-containing groups on graphene oxide benefit to the adsorption of Al-(OC₃H₇)₃ (aluminum isopropoxide), leading to the uniform dispersion of rGO with Al₂O₃ which is hydrolyzed from aluminum isopropoxide in solvothermal reactions. Further, this research methodology has been extended to another ceramics-graphene nanostructure assembly, i.e., silica-rGO hybrids, by optimizing experimental conditions for the hydrothermal and hot pressing process. This book chapter will be a significant contribution for the applications of ceramics-graphene assembly nanomaterials, which can be made by simple fabrication route and which can be further applied as electrolytes, catalysts, conductive, electrochemically active, and as dielectric materials for the high-temperature applications due to enhanced physical properties.

Keywords: graphene, ceramics, enhanced physical properties, solvothermal, hot pressing, calcination, hydrolyzed, platelets, reduced graphene oxide, thermal properties, electrical properties, dielectric properties, mechanical properties

1. Introduction

In recent years, hybrid nanostructures have achieved great technological interest, because of the ability of the nanostructures which intends to design and manufacture hybrid materials with enhanced physical properties [1, 2]. For a desired technological application, various excellent properties can be combined into a single hybrid nanostructure, this is an excellent feature of the hybrid nanostructures. Moreover, in hybrid nanostructures, the enhanced electronic interactions among various types of components are possible, which is the main reason to enhance the physical properties of hybrids [3, 4]. In ceramics-graphene hybrids, enhanced physical properties can be used in the high electrical, mechanical, and thermal applications, because of higher electrical conductivity, thermal conductivity, dielectric and better mechanical properties [5]. Due to the versatile physical and chemical properties [6, 7], graphene has opted in huge scientific activities in

progress of research and development for the field of science and technology. The combination of suitable electrical, mechanical, thermal, and physical properties can apply not only for a broad spectrum of applications but also as a basic essential unit for the fundamental and advanced technological research [8, 9]. In hybrids or composite, scientists worldwide have been impressed by the unique combination of individual physical properties of graphene [8], that makes graphene an ideal option, or as an advanced component in both the hybrids as well as composites. For monolithic ceramics, in particular, physical properties of graphene have been researched and investigated as an ideal component in the monolithic ceramics-graphene hybrids or composite [10, 11]. Due to the higher strength, stiffness, and high-temperature stability, monolithic ceramics are used and known commonly as a very promising structural material for mechanical and high-temperature applications [12, 13]. But the field of application is still vacant due to mechanical unreliability, and very lower electrical conductivity, and limited physical properties of the monolithic ceramics.

Due to graphene's extraordinary physical properties [14, 15], incorporating graphene in the ceramics can have great potential for electro-conductive, and high mechanical applications. In graphene-ceramics hybrids, enhanced physical properties could be implemented in a wide range of the material related applications in the field of aerospace, processing industries, and military based applications. [16, 17] In view of the fabrication routes [17, 18], development of the graphene ceramic hybrids is still complicated due to reinforcement particle at a very nanometric scale. For fabrication methodology, practical issues can be classified into wide categories such as (1) in ceramic nanostructures, homogenous dispersion of the graphene is important for enhanced physical properties; (2) easy processing route of graphene-ceramics hybrids or nanocomposites is necessary; (3) interfacial bonding and interaction between graphene and ceramic nanostructures are very important as it directly reduces the physical properties of the graphene-ceramics hybrids or nanocomposites. For ceramics-graphene hybrids, uniform dispersion of the graphene in the ceramic matrices is an important factor [12]. Due to the high surface area of graphene [8], proper graphene dispersion is a very important factor, which further ensures efficient load transfer between graphene and available ceramics nanostructures in the hybrids. This is major concerns during the incorporation of graphene in the ceramics, due to the higher surface area of graphene [6]. For this purpose, scientists have used various dispersing agents [19, 20]. The use of dispersing agent gives rise to higher surface potential, double layer formation, as well possibility of strong electrostatic repulsion, which helps to uniform dispersion of graphene in graphene-ceramics hybrids. Mechanical dispersion of graphene is possible through many routes such as ultra-sonication, ball milling, and stirring [7, 21].

The enhanced physical properties of graphene-ceramic materials depend upon many factors such as thin layers of graphene, fine particles size and phase homogeneity [22]. For graphene-ceramics hybrids, well aligned and controlled nanostructures are important in toughening of hybrids. In literature, there are available many fabrication ways of graphene-ceramics hybrids such as powder processing, colloidal processing and sol-gel fabrication. In most of the work on graphene-ceramics by conventional powder routes, physical properties are not as good as expected because graphene is prone to agglomeration due to van der Waals forces. Therefore, in this chapter, our focus is on new solvothermal-hot press method, which is used to fabricate alumina-rGO, and silica-rGO hybrids, with a systematic study on enhanced physical properties of the hybrids for efficient application. In hybrids, the physical properties are enhanced by a great degree, because of use of calcination conditions, as well as the hot-pressing conditions. The two structural ceramics, which we will discuss in this chapter, are alumina and silica, respectively.

Ceramics usually have a brittle attribute with low strength [11]. Among many ceramics, alumina is one of the widely used structural ceramic due to the shaping capability, and the good thermal conductivity [12]. Alumina has applications in the field of high-speed cutting tools, dental implants and insulators [13, 14]. To improve the mechanical properties, carbon nanotubes have been used to enhance the fracture toughness (by a degree of 94%), hardness (by a degree of 13%), and flexural strength (by a degree of 6.4%) of the alumina [15]. Ball-milled alumina/zirconia/graphene composite has been investigated with 40% enhanced fracture toughness by adding the graphene platelets [16]. In another work, alumina-rGO nanocomposites have been fabricated by the dry sol-gel method, from which it was indicated that BET surface area of rGO is essential to enhance the surface charge properties of hybrids [17]. In another work, alumina-graphene composite films have been reported with low optical gap (1.53 eV) [18]. Alumina-rGO nanocomposite by in-situ deposition have shown morphologies of nanoparticles of alumina structures on rGO with BET surface area of $242.4 \text{ m}^2 \text{ g}^{-1}$ and the low porosity [19]. Alumina/rGO/poly(ethylenimine) composite has been used to capture carbon dioxide from the flue gas [20]. In a microwave preparation of alumina-rGO composites, the grain size of alumina matrix was reduced to 180 nm compared to 475 nm of the conventional sintering process, leading to an increase in Young's modulus of 180 from 148 GPa under the same measurement condition [21]. In this chapter, we will discuss the preparation of hybrids consisting of $\gamma\text{-Al}_2\text{O}_3$ nanorods and rGO by a solvothermal method. This solvothermal method is used to form hybrids composed of cross-linked $\gamma\text{-Al}_2\text{O}_3$ nanorods and reduced graphite oxide (rGO) platelets. With further hot pressing, a hybrid monolith has been made for the systematic study on enhanced physical properties of the hybrids.

The second structural ceramics, which we will discuss in this chapter, is silica. Among various kinds of the ceramics, silica particles are one of the widely used additive ceramic due to its functionalized ability and stability with a range of materials [23, 24]. Silica has various applications in the domain of polymer, biomedical, and composite engineering [25]. To improve the physical properties, rGO has been used to enhance thermal conductivity ($0.452 \text{ Wm}^{-1} \text{ K}^{-1}$), storage modulus (3.56) and dielectric constant (77.23) of epoxy/SiO₂/rGO hybrid [26]. In another work, in-situ sol-gel processed silica nanoparticles decorated with graphene oxide sheets are obtained, from which it was found that presence of rGO is essential to improve the corrosion resistance, dispersion, and the barrier properties of hybrid [27]. In another work, SiO₂-graphene hybrids have shown superior gas sensing response (31.5%) towards 50 ppm NH₃ for 850 s, in comparison to rGO based sensor (1.5%) [28]. Using one-step hydrothermal method, SiO₂-rGO nanohybrid has shown comparatively better BET surface area ($676 \text{ m}^2 \text{ g}^{-1}$) and 98.8% Cr(VI) adsorption efficiency [29]. SiO₂ supported polyvinylidene fluoride has shown high dielectric constant (72.94) and low dielectric loss (0.059), which is due to the addition of ultrathin graphene [30]. Among the field of diverse inorganic particles, still, there is need to do much of scientific research for enhanced physical properties of silica-carbon based hybrids.

2. Experimental setup/fabrication route for ceramics-graphene hybrids

There are many fabrication methods for graphene-ceramics materials. Here in this chapter, In brief, the preparation of ceramics-graphene hybrids was done by mixing GO with cyclohexane and corresponding metal alkoxide followed by a solvothermal reaction. For the preparation, 0.1 g of GO was firstly dispersed in 35 ml cyclohexane, after which desired amount of corresponding metal alkoxide was

added drop by drop to the GO suspension above. Centrifugation was used to separate the products which were then washed out several times with cyclohexane. The solid samples thus obtained are denoted as (Ceramics Oxide)_x/GO. (Ceramic Oxide)_x/GO was dispersed again in 50 ml cyclohexane and then transferred to a 100 ml Teflon-lined stainless-steel autoclave for hydrothermal reaction. After the reaction was carried out, samples denoted as (Ceramic Oxide)_x/rGO. (Ceramic Oxide)_x/rGO was then calcinated at a temperature above 700 K for a specific interval of time to form Ceramics Oxide/rGO hybrids. Graphene-ceramics hybrid powder containing different wt.% of rGO were obtained using the same method. Hot pressing of ceramics-graphene hybrid powder was performed in a vacuum furnace (model number OTF-1200X-VHP4). The flowchart fabrication scheme of gamma alumina-rGO hybrid with detailed experimental conditions is represented in **Figure 1**.

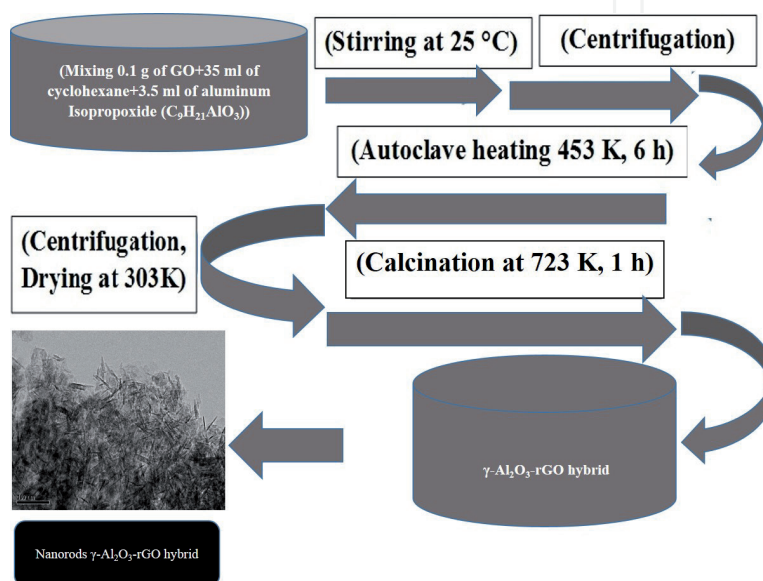


Figure 1.
Flow chart fabrication scheme for γ - Al_2O_3 -rGO hybrids.

Graphical abstract

After calcination and hot-press processing, monolithic sphere of SiO_2 and rGO platelets hybrids are obtained with Improved Physical Properties

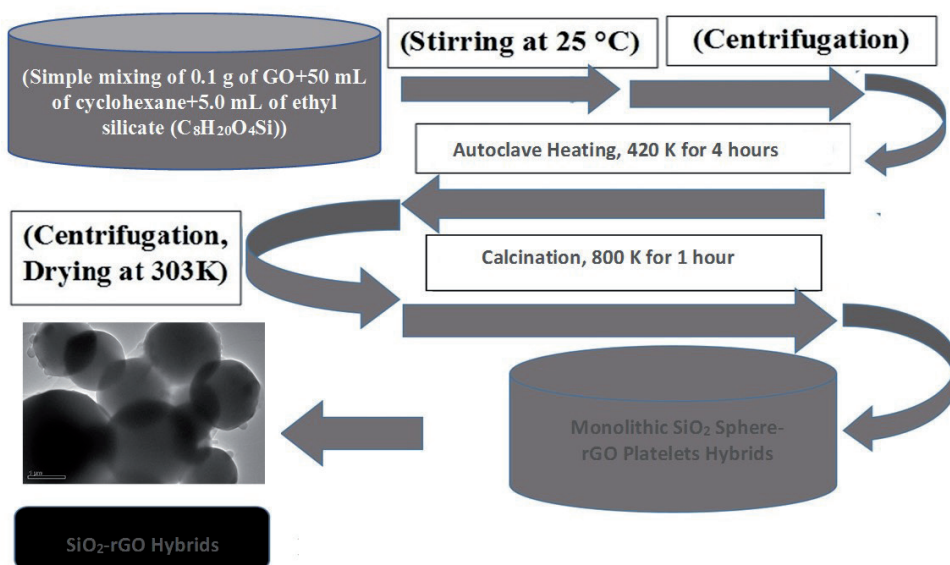


Figure 2.
Flow chart fabrication scheme for SiO_2 -rGO hybrids.

Figure 2 shows the fabrication flowchart of silica-rGO hybrids, which are obtained using specific temperature and hot pressing conditions.

3. Physical properties of alumina-graphene hybrids for technological and applied applications

TGA (shown in **Figure 3**) of γ -Al₂O₃-rGO powder samples show that different calcination times has led to different concentrations of rGO in the hybrids. The TGA curves of all hybrids show a stable weight loss between 400 and 600°C, as a result of the removal of all carbon-related materials, and other impurities (if any) after heating these hybrids to 800°C in an air atmosphere. For the samples with 3-, 2- and 1-h calcination time, the 7.705, 12.830 and 16.707 wt.% loss were calculated. For 1-h sample, the unique weight loss is observed.

SEM image in (**Figure 4a**) for bare Al₂O₃ shows particles like morphology. The size of particles has ranged from 500 nm to few micrometers. TEM image in (**Figure 4b**) shows elongated nanocrystals or nanorods of bare Al₂O₃. Sample before calcination but after autoclave heating has been referred as Al(O)_x/rGO. SEM image of Al(O)_x/rGO after heating in an autoclave at a temperature of 453 K for 6 h but before calcination is shown in the **Figure 4c**. Even after calcination at 723 K for 2 h, the SEM image in **Figure 4d** shows the same particle like morphology but size of particles has ranged from 1 micrometers to few micrometers. TEM image of γ -Al₂O₃-rGO hybrids after calcination at 723 K for 2 h is shown in the **Figure 4e**. It shows elongated and fine nanorods of γ -Al₂O₃ with rGO layer in hybrids. The TEM image in **Figure 4e** indicates the presence of a very thin rGO layer, which acts as a continuum matrix in these hybrids.

The presence of rGO can also be confirmed by closely observing **Figure 4e**. In this figure, low-contrast features are actually edges or small portions of the graphene sheet (**Figure 4e**) on which γ -Al₂O₃ is uniformly distributed in dense concentrations. Further, the selected area electron diffraction pattern presented in **Figure 4f** shows the inter-planar spacing's of D = 0.175 nm and D = 0.151 nm, corresponding to the (200) and (111) planes of γ -Al₂O₃. The fabrication of the γ -Al₂O₃ phase was

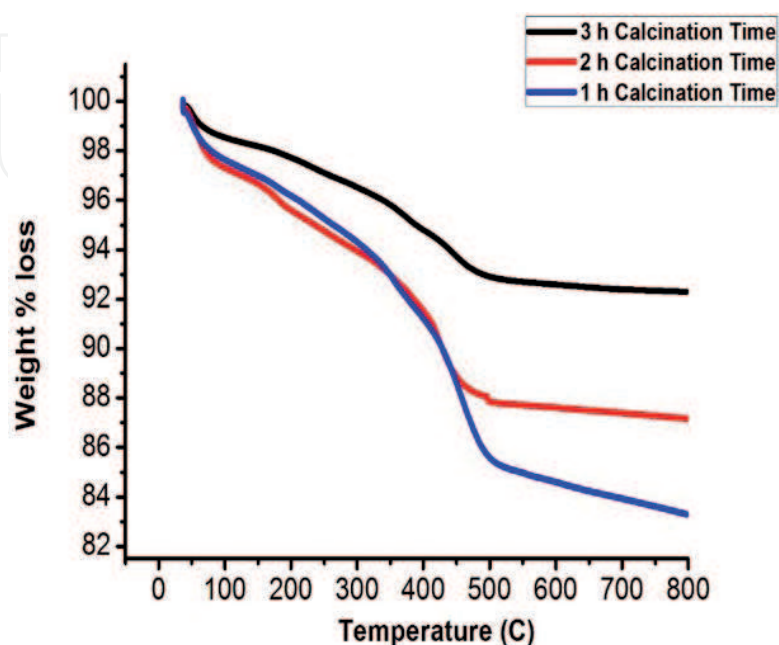


Figure 3. TGA curves of γ -Al₂O₃-rGO hybrids using calcination time of 1, 2 and 3 h in air atmosphere up to 800°C.

confirmed from the XRD results as shown in **Figures 5 and 6**, respectively. The inset of **Figure 6** shows the XRD of a sample without GO ($\gamma\text{-Al}_2\text{O}_3$). In the XRD spectra of all three samples with calcination times of 1, 2, and 3 h, the presence of characteristic peaks of $\gamma\text{-Al}_2\text{O}_3$ is evident and (matched with JCPDS card no. 10-0425). Further, a relatively broad nature of sharp peaks is observed in the XRD of $\gamma\text{-Al}_2\text{O}_3$ and rGO hybrids (after calcination, **Figure 5**) and in the inset of **Figure 6** (for pure $\gamma\text{-Al}_2\text{O}_3$). This suggests a nanocrystalline structure of $\gamma\text{-Al}_2\text{O}_3$ with nanorod morphology, which is also quite evident from the TEM images (**Figure 4e**).

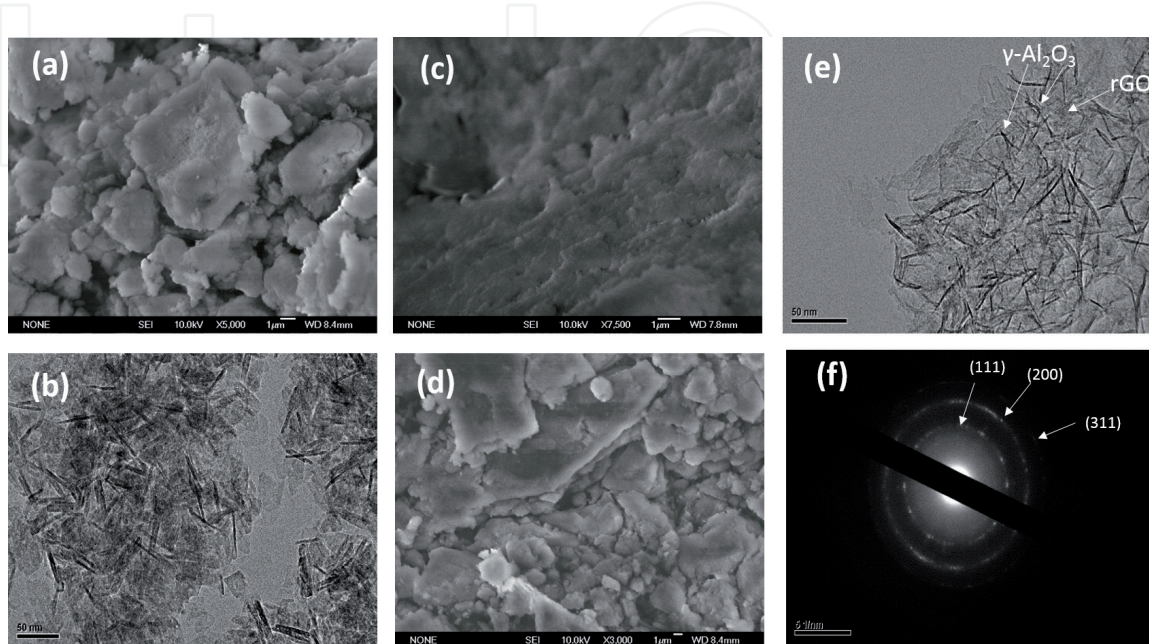


Figure 4. (a) SEM and (b) TEM images of pure $\gamma\text{-Al}_2\text{O}_3$, SEM images of $\text{Al}(\text{O})_x/\text{GO}$ (c) before calcination at autoclave heating of 453 K for 6 h and (d) after calcination at 723 K for 2 h. (e) TEM image of $\gamma\text{-Al}_2\text{O}_3$ -rGO after calcination at 723 K for 2 h, and (f) SAED pattern of $\gamma\text{-Al}_2\text{O}_3$ -rGO hybrid at 723 K for 2 h.

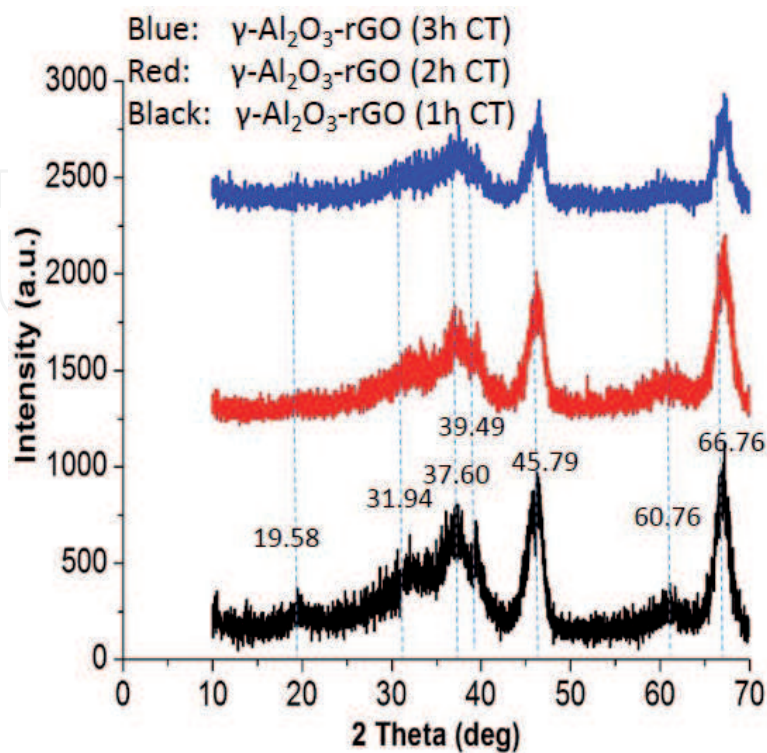


Figure 5. XRD of $\gamma\text{-Al}_2\text{O}_3$ -rGO (1-h calcination time), $\gamma\text{-Al}_2\text{O}_3$ -rGO (2-h calcination time) and $\gamma\text{-Al}_2\text{O}_3$ -rGO (3-h calcination time).

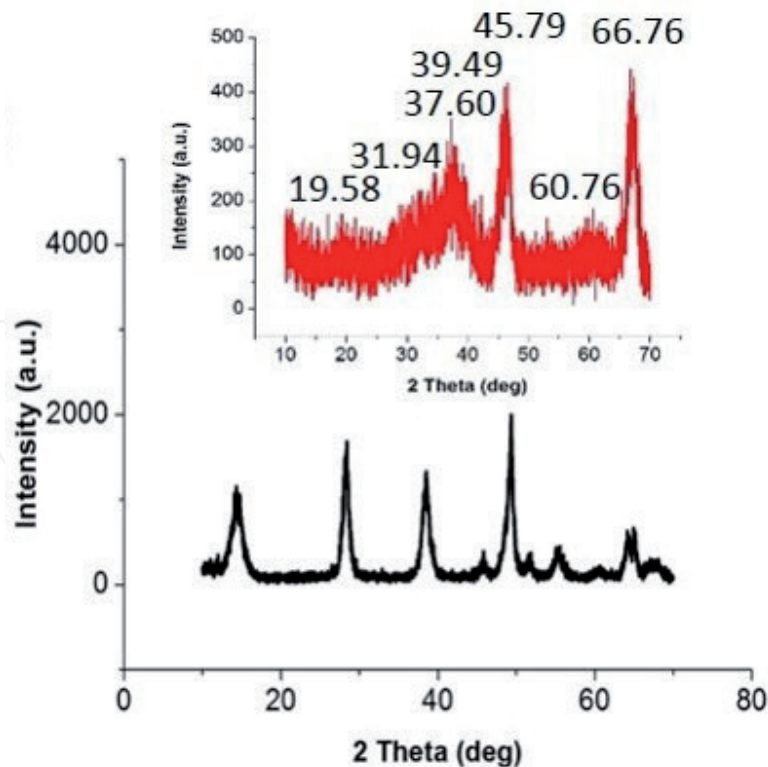


Figure 6.
XRD of γ -Al₂O₃-rGO before calcination and inset is XRD of pure γ -Al₂O₃, fabricated at 723 K.

In all cases after calcination for 1, 2 and 3 h in **Figure 5**, the characteristic peaks of GO that usually appear at 10.28 are also invisible in these hybrids. The total changes in the peaks of the XRD pattern before and after calcination indicate the effects of hydrothermal and calcination treatments.

Raman spectroscopy is conducted on these hybrids to confirm the presence of carbon, shown in **Figure 7**. The Raman spectra of the sample indicate that rGO is present in hybrids with 1-, 2- and 3-h calcination time. For calcinated samples with different times (1, 2, and 3 h), the Raman intensity decreases with calcination time, consistent with TGA results. The G-band value is different in the Raman spectrum of all γ -Al₂O₃ and rGO hybrids as compared to pristine graphene. This reveals the presence of prominent electronic interactions between γ -Al₂O₃ and rGO in hybrids.

The nanohybrids of γ -Al₂O₃-rGO with 3, 2, and 1-h calcination time have BET surface areas of 361, 408, and 379 m²·g⁻¹, respectively. For bare γ -Al₂O₃, the BET surface area is 280 m²·g⁻¹. The bulk densities of γ -Al₂O₃-rGO with 3-, 2-, and 1-h calcination time have values of 1.61, 1.37, and 0.92 g cm⁻³, respectively. For bare γ -Al₂O₃, the bulk density is 2.75 g cm⁻³. Clearly, the presence of rGO has led to high BET surface-area values. Presence of rGO in hybrid can increase the BET surface area, pore volume, and thermal conductivity. The higher surface areas, pore volume, thermal and electrical conductivity are significant factors from an applied application point of view. Further as the calcination temperature increased, the crystallinity of γ -Al₂O₃ and rGO hybrids was considerably enhanced as shown in the XRD of γ -Al₂O₃ and rGO hybrids which are taken from 500 to 800 K as in **Figure 8**. For the analysis, calcination time is kept constant (1 h) and further calcination temperature was set as 500, 600, 650, 700, 750, and 800 K, respectively. Actually, most of the samples do not show any characteristics peaks for the rGO in XRD (**Figure 8**).

Now, the crystallinity of γ -alumina is a major concern. Further, it is found that sharp, broad and prominent peaks are obtained for γ -alumina at the higher calcination temperature. But the peaks were weaker or not prominent, when there was a lower calcination temperature such as 500, 600, and 650, respectively.

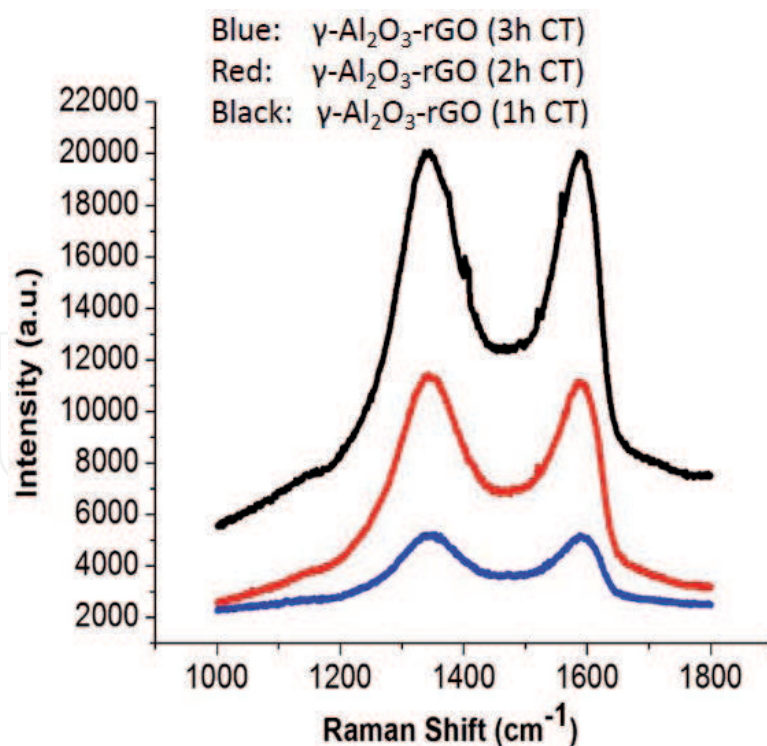


Figure 7. Raman spectra of $\gamma\text{-Al}_2\text{O}_3\text{-rGO}$ (1-h calcination time), $\gamma\text{-Al}_2\text{O}_3\text{-rGO}$ (2-h calcination time) and $\gamma\text{-Al}_2\text{O}_3\text{-rGO}$ (3-h calcination time).

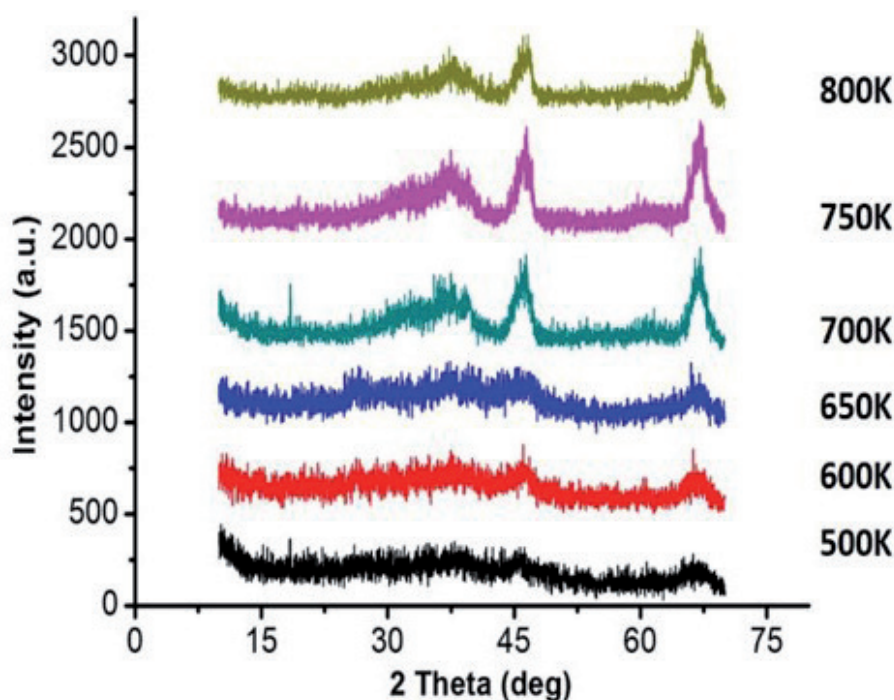


Figure 8. XRD of $\gamma\text{-Al}_2\text{O}_3\text{-rGO}$ hybrids taken from 500 to 800 K.

Hot-pressed $\gamma\text{-Al}_2\text{O}_3$ and rGO nanohybrid samples were fabricated at a temperature of 900°C . Hot pressing can affect the quality of graphene. Preserving the quality of graphene as much as possible is a major factor in the enhanced properties of graphene hybrids [19–21]. The SEM morphology of all samples after hot pressing is shown in the **Figure 9**.

The Raman and XRD data for $\gamma\text{-Al}_2\text{O}_3\text{-rGO}$ calcinated at 2 h, before and after hot pressing, are shown in **Figures 10** and **11**, respectively. Before hot pressing,

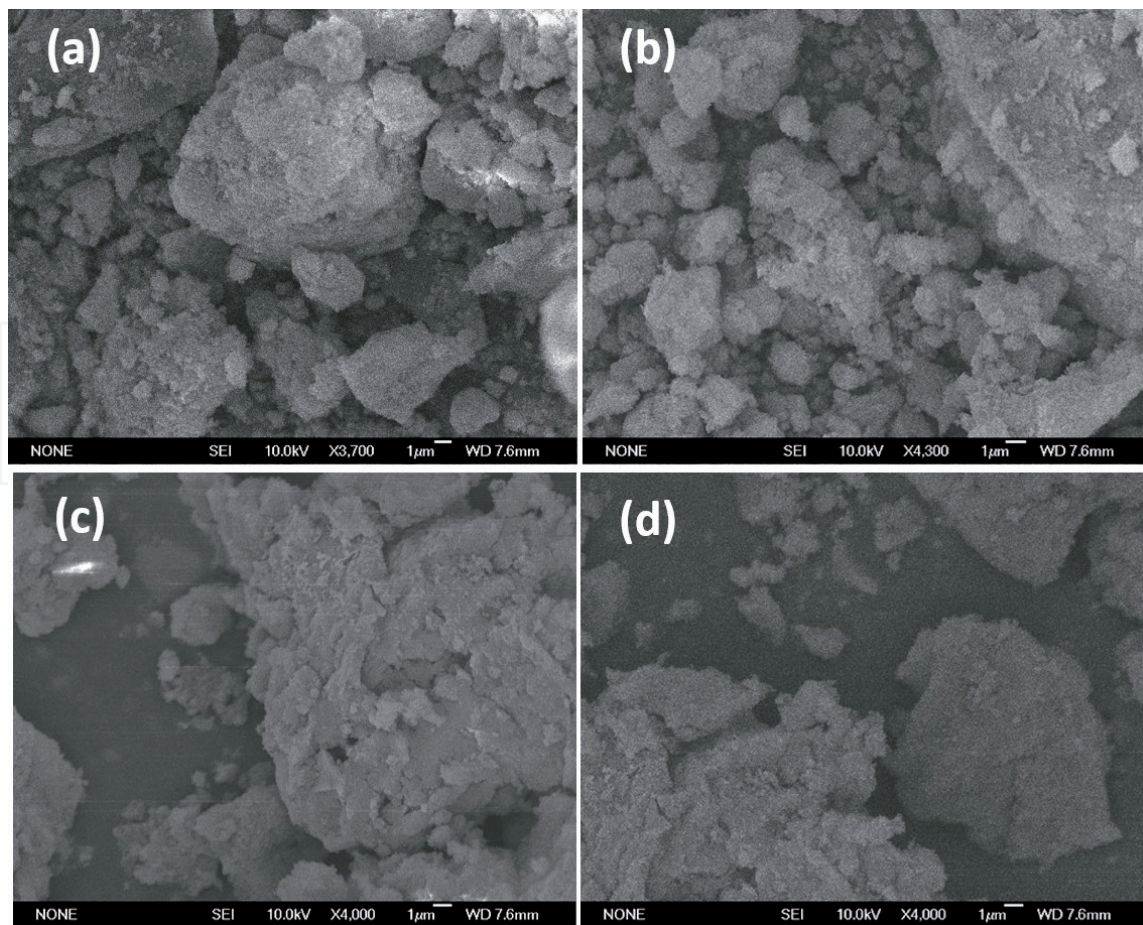


Figure 9. SEM images of hot pressed samples (a) γ - Al_2O_3 -rGO (1 h calcination time), (b) γ - Al_2O_3 -rGO (2-h calcination time), (c) γ - Al_2O_3 -rGO (3-h calcination time), and (d) pure γ - Al_2O_3 (1-h calcination time).

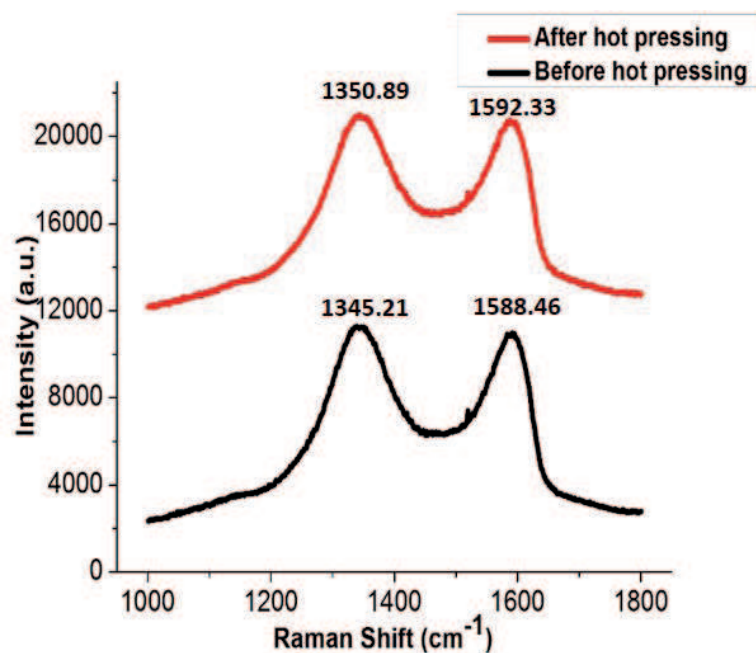


Figure 10. Raman of γ - Al_2O_3 -rGO (2-h calcination time) before and after hot-pressing.

the D band for the sample is found at 1345.21 cm^{-1} . After hot pressing, it is found at 1350.89 cm^{-1} . Before hot pressing, the G band is found at 1588.46 cm^{-1} . After hot pressing, the G band is found at 1592.33 cm^{-1} . This shift in D and G bands is due to the electronic interaction between γ - Al_2O_3 and rGO during hot press processing.

There is not much effect on the integrity of alumina nanorods during hot pressing as this is also confirmed by XRD (**Figure 11**).

The three hot-pressed samples of γ - Al_2O_3 -rGO hybrids with calcination times from 1, 2, and 3 h and pure γ - Al_2O_3 (calcinated at 1 h) were studied for properties studies. Electrical conductivity as a function of the concentration of rGO in the hybrid is shown in the **Figure 12**.

It is also found that the electrical conductivity increases with more rGO content. The electrical conductivities of γ - Al_2O_3 -rGO calcinated at 1, 2, and 3 h were 8.2×10^1 , 7.8×10^1 , and $6.7 \times 10^1 \text{ S}\cdot\text{m}^{-1}$, respectively. There is conductivity ($5.1 \times 10^{-10} \text{ S}\cdot\text{m}^{-1}$) found in bare γ - Al_2O_3 samples, which confirms that the bare alumina is highly non-conductive. Previous reports show that little carbon (2%) in alumina-carbon hybrids can enhance conductivity up to great level (from $10^{-12} \text{ S}\cdot\text{m}^{-1}$ to $10^{-1} \text{ S}\cdot\text{m}^{-1}$). The improvement of the electrical properties is due to heat treatment, and it has been attributed to mechanisms such as restoration of sp^2 C—C bonds and cross-linking between reduced GO sheets during the thermal annealing process [28]. These

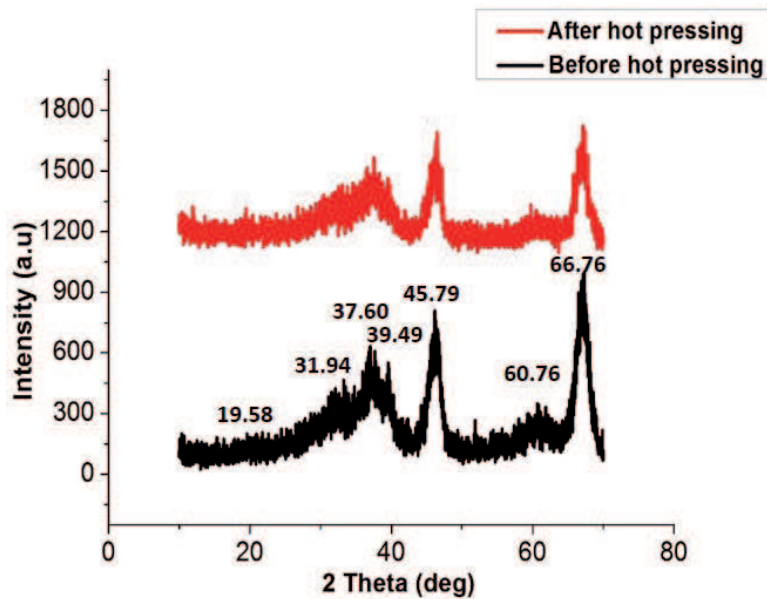


Figure 11.

XRD of γ - Al_2O_3 -rGO (2-h calcination time) before and after hot pressing.

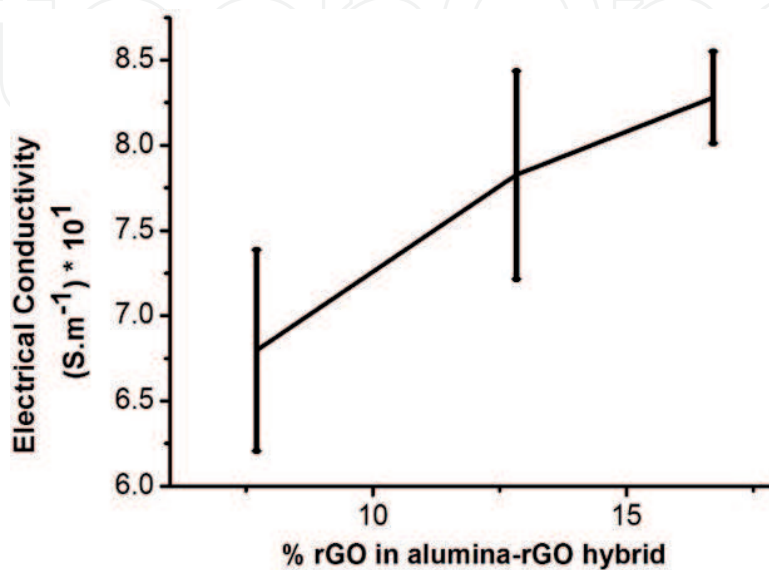


Figure 12.

Electrical conductivity vs. % rGO with error bar.

samples showed a significant increase and improvement in thermal conductivity. This is mainly because of the excess surface electrons and the layered structure of rGO. Thin rGO layers can independently have higher conductivities. The thermal conductivity of pure alumina was reported $0.5 \text{ Wm}^{-1} \text{ K}^{-1}$ at 75°C , which prepared by hydrolysis and solvothermal method. The thermal conductivity of $\gamma\text{-Al}_2\text{O}_3\text{-rGO}$ with 1-, 2- and 3-h calcination time and bare $\gamma\text{-Al}_2\text{O}_3$ (1-h calcination time) as a function of varying temperatures is shown in **Figure 13**. At a room temperature of 25°C , the thermal conductivities of pure $\gamma\text{-Al}_2\text{O}_3$ and $\gamma\text{-Al}_2\text{O}_3\text{-rGO}$ (3, 2 and 1-h calcination time) were found to be 0.81, 1.4, 2.37, and $2.53 \text{ Wm}^{-1} \text{ K}^{-1}$, respectively. As the temperature was increased, the thermal conductivity gradually increased in all hybrids of $\gamma\text{-Al}_2\text{O}_3\text{-rGO}$ and bare $\gamma\text{-Al}_2\text{O}_3$.

In the case of ceramic materials, porosity is one of the main reasons for decreases in the overall thermal conductivity. The dielectric properties of $\gamma\text{-Al}_2\text{O}_3\text{-rGO}$ hybrids and bare $\gamma\text{-Al}_2\text{O}_3$ were measured using an LCR meter, as shown in **Figure 14**. For $\gamma\text{-Al}_2\text{O}_3$, its dielectric constant is found to be around 9.8, which is closer to that of pure alumina.

For the 3-h calcinated hybrid, the dielectric constant is significantly increased and is multiplied by a factor of 12, which indicates the presence of a first percolation threshold. However, when the rGO content is enhanced in the hybrids by decreasing calcination time to 2 h, the dielectric constant further decreases and approaches the value of pure $\gamma\text{-Al}_2\text{O}_3$. This is attributed to an anomalous trend that produces drastic changes that are usually suffered by most ceramic materials and matrix microstructures. By further decreasing the calcination temperature of hybrids to 1 h, the dielectric constant increases by four orders of magnitude, which indicates the presence of a second percolation threshold that is achieved through this higher value of dielectric constant. Similarly, the dielectric loss indicates very similar behavior in the real part of the dielectric constant as shown inset of **Figure 14**. Dielectric loss of $\text{Al}_2\text{O}_3\text{-rGO}$ hybrid with 1-h calcination time is much increased, as more rGO in hybrid and this more rGO can make conductive layers' network of rGO in between alumina nanorods; this would cause significant leakage current, and thus result in a high dielectric loss. The existence of a double percolation threshold in such $\gamma\text{-Al}_2\text{O}_3$ and rGO hybrids can be significant for technological and applied applications because it can be used to enhance the dielectric properties in $\gamma\text{-Al}_2\text{O}_3$ and rGO

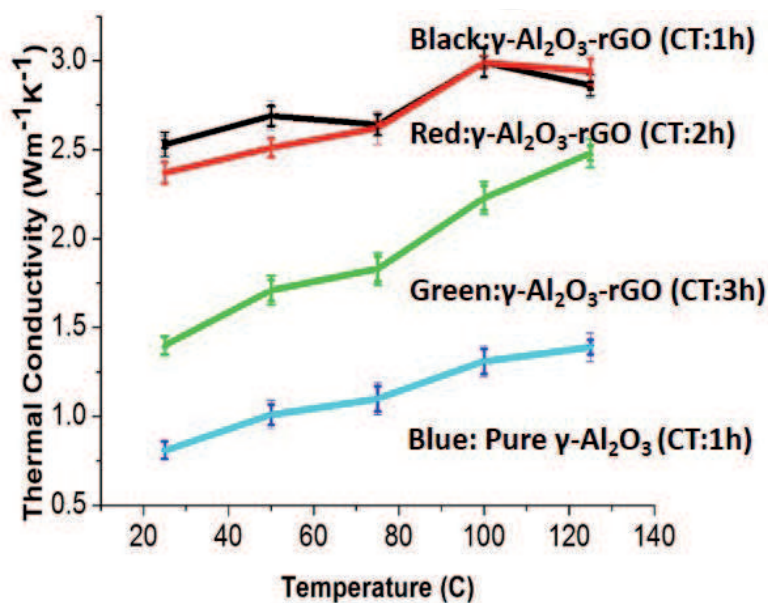


Figure 13. Thermal conductivity as function of temperature (black, red and green curves are for $\gamma\text{-Al}_2\text{O}_3\text{-rGO}$ with 1-, 2- and 3-h calcination time with error bar.

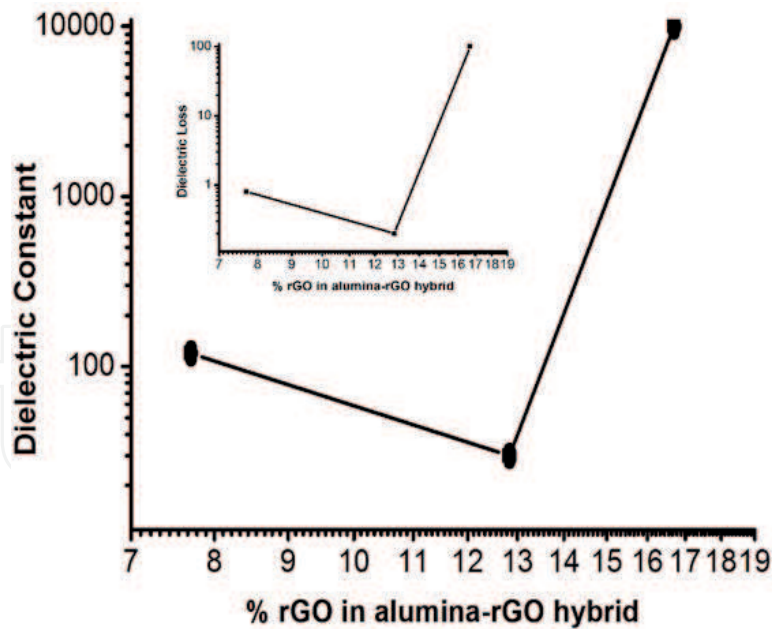


Figure 14.
Dielectric properties vs. % rGO in γ -Al₂O₃-rGO hybrid with error bar.

hybrids with the addition of a small rGO % in the hybrid. From compressive and tensile stress-strain analysis, it is evident that with an increase of rGO content in the hybrid the mechanical compressive and tensile strength is increased as compared to pure alumina. This further caused more strength in alumina hybrids, i.e., higher compressive, tensile strength and higher compressive young modulus values for these hybrids (**Figures 15 and 16**). The enhanced mechanical properties of γ -Al₂O₃ and rGO hybrids can be attributed to covalent interaction of rGO with γ -Al₂O₃ and to efficient load transfers between rGO and nanorods of γ -Al₂O₃. Further, this is closely bound with the elongated and fine γ -Al₂O₃ nanorods and atomic-level rGO layers with a covalent interaction with γ -Al₂O₃. Young modulus of γ -Al₂O₃-rGO with 1-, 2- and 3-h calcination time and γ -Al₂O₃ with 1-h calcination time are calculated as 3.7, 3.2, 2.65 and 1.80 GPa. In this case, lower tensile and compressive strength in alumina can be due to the availability of powder instead of single crystals of alumina. Increase in calcination temperature has reduced wt.% of rGO in a hybrid. This is the reason of having more strength in hybrids with lower calcination

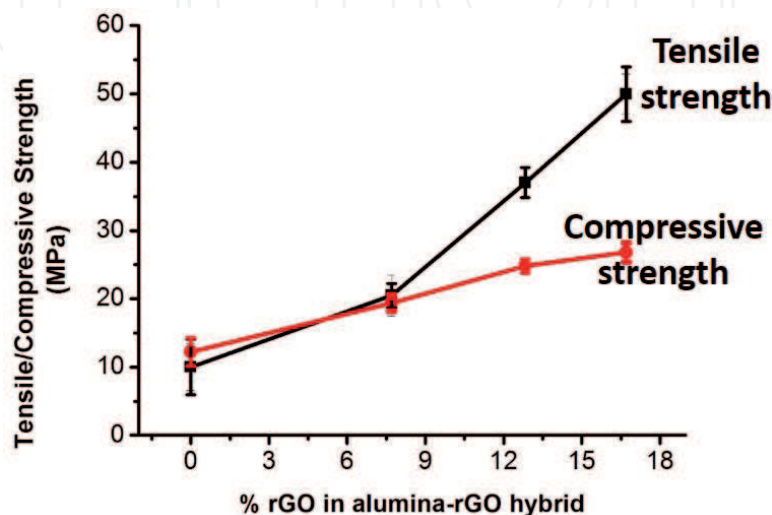


Figure 15.
Compressive and tensile strength as a function of rGO for hybrid γ -Al₂O₃-rGO with error bars.

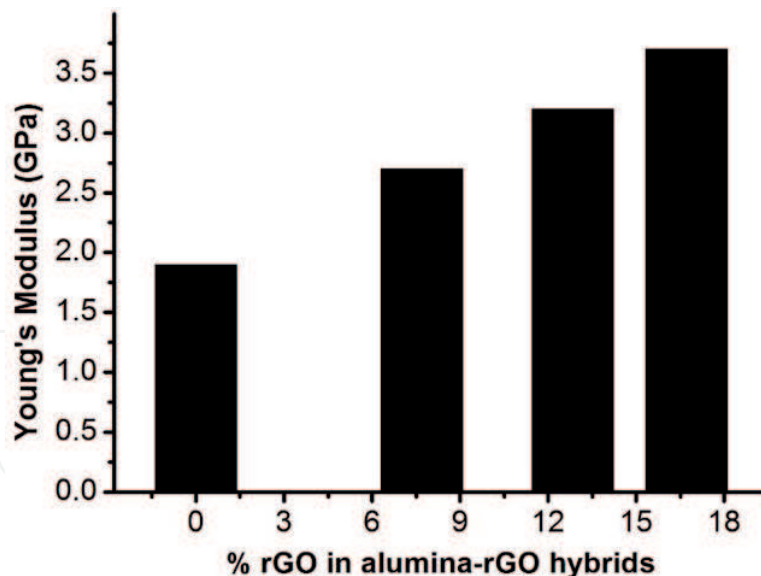


Figure 16.
Compressive Young's modulus as % rGO in alumina-rGO hybrids.

temperature. The maximum value of Young's modulus (3.7 GPa) is determined in 1-h calcinated alumina-rGO hybrid, as also shown in **Figure 16**.

Thus, elongated dimensions of nanorods are a major cause of higher mechanical strength in these hybrids. In γ - Al_2O_3 -rGO monoliths, higher calcination temperature enhances length, diameter and aspect ratios of γ - Al_2O_3 nanorods. Presence of more rGO and higher aspect ratio elongated alumina rods determines the interface interaction between rGO platelets and alumina. A 90% increase in tensile strength and 75% in compressive strength occurs when the content of rGO is increased from 0 to 7.705 wt.% in the hybrid calcination of a hybrid at 3-h processing time. With the increase of rGO, alumina-rGO hybrids have shown higher values for young modulus. The hybrids with 1-h calcination time show good enhancement in its electrical conductivity ($8.2 \times 10^1 \text{ S m}^{-1}$) due to the availability of more surface electrons of rGO. This is best-reported values for conductivity. After hot press process, there is a wide increase in electrical conductivity values when there is a decrease of calcination temperature from 3 to 1-h processing time in these hybrids. Further, the thermal conductivity of γ - Al_2O_3 -rGO is enhanced by more than 80% compared to that of bare γ - Al_2O_3 when there is an increase in rGO content up to 7.705 wt.% in γ - Al_2O_3 and rGO hybrids. There is a 77% increase in thermal conductivity using this solvothermal method in these γ - Al_2O_3 and rGO hybrids. Physical properties such as the BET surface area and bulk density are also improved. Elongated dimensions of nanorods are a major cause of higher mechanical strength in these hybrids. Dielectric constant increases by four orders of magnitude through second percolation threshold with the addition of small rGO in a hybrid. Enhancement in physical properties can be due to well aligned, elongated and fine nanorods morphology of alumina in hybrids, calcination, and hot press processing further played an important role by sustaining quality rGO in hybrids. These nanohybrids of alumina monoliths and rGO can be further applied as catalysts, electrolytes, and as electrochemically active materials because of their nanometer dimensions and enhanced physical properties.

4. Physical properties of silica-graphene hybrids for technological applied applications

With rGO in the SiO_2 -rGO hybrids, the hybrids powder shows a prominent change in the color after calcination. TGA of SiO_2 -rGO powder samples shows that

different initial GO suspensions (0.1, 0.2, and 0.3 g) have led to different concentrations of rGO in the hybrids. The TGA curves of all hybrids show a stable weight loss up to 100°C, as a result of moisture loss and between 150 and 300°C, as a removal of unreduced GO functional groups, and from 350 to 600°C, as a result of removal of all carbon related materials which are due to the decomposition of rGO, and other impurities (if any) after heating SiO₂-rGO hybrids to 800°C in an air atmosphere. By keeping 1-h calcination time, with initial 0.1 g GO suspension in hybrid, the wt.% loss of 1.55 was calculated. With initial 0.2 g GO suspension in hybrid, the wt.% loss of 6.75 was calculated. With initial 0.3 g GO suspension in hybrid, the wt.% loss of 10.82 was calculated. From the wt.% loss, it is found that % rGO is determined as 1.55, 6.75 and 10.82 in the SiO₂-rGO hybrids, which are obtained from 0.1, 0.2 and 0.3 g GO suspensions, respectively. All powder samples before calcination (at 800 K for 1 h) but after autoclave heating (at 420 K for 4 h) have been referred to as Si(O)_x/rGO. Lower and higher magnification SEM images for hybrid SiO₂-rGO-1.55% (calcinated at 800 K for 1 h) are shown as in **Figure 17a** and **b**. From SEM images, it is clear that SiO₂ have sphere morphology with location side by side along with overlapping and wide size distribution of spheres, ensuring very close contact among SiO₂ spheres in the whole network. The diameters of spheres have variation in size ranging from 5 nm to 3 μm. Bare SiO₂ particles (calcinated at 800 K for 1 h) have shown spherical morphology with the little rough surface as shown in the **Figure 17b** and **d**. The rough texture of SiO₂ sphere is confirmed by the closely looking to **Figure 17d**. Diameters of SiO₂ spheres vary in size from 1 μm to a few micrometers. TEM is carried out to verify the morphology, which is obtained in SEM. Further, TEM image of SiO₂-rGO-1.55% shows that the SiO₂ spheres were uniformly encapsulated by the thin layers of rGO (marked with an arrow) as in the **Figure 17e**. After hydrothermal (420 K for 4 h) and calcination (800 K for 1 h) treatments, in SiO₂-rGO-1.55% hybrid, the SiO₂ spheres is fully decorated with small rGO sheets.

In **Figure 17e**, the low-contrast features are small portions of the graphene layers on which SiO₂ spheres are uniformly distributed. After thermal treatments, uniform distribution of SiO₂ spheres and rGO sheets is the main factor for enhanced properties of the SiO₂-rGO hybrid. TEM image of SiO₂-rGO-1.55% is shown in the

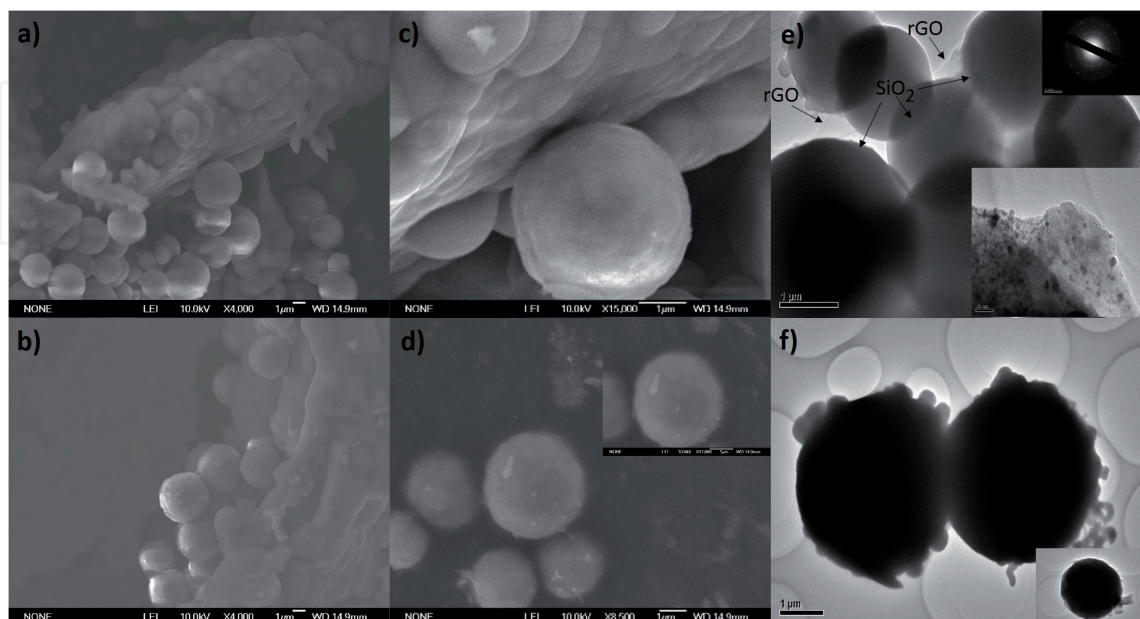


Figure 17.

SEM images of (a) SiO₂-rGO-1.55% (b) pure SiO₂ fabricated at a calcination temperature of 800 K for 1 h at lower magnification. SEM images of same (c) SiO₂-rGO-1.55% (d) pure SiO₂ at higher magnification. (e) TEM images of same SiO₂-rGO-1.55% at lower magnifications, inset is SAED pattern for same sample and (f) TEM images of same pure SiO₂ at higher magnifications.

Figure 17e, from TEM image it is evident that diameters of SiO₂ spheres ranges from few nanometers to few micrometers, and agreed with SEM results. For the SiO₂-rGO-1.55% hybrid, the selected area electron diffraction (SAED) pattern is presented in the inset of **Figure 17e**, and it shows the hybrid is composed of SiO₂ spheres and thin rGO layers. In SAED pattern, the electron diffraction rings indicate the amorphous nature of SiO₂. Rough texture and the non-uniform surface of a pure SiO₂ sphere are confirmed from TEM results in **Figure 17f**. Diameters of spherical SiO₂ vary from 1 μm to a few micrometers as evident from TEM characterization (**Figure 17f**, and in agreement with SEM results of **Figure 17b** and **d**. For more insight into structural properties of SiO₂-rGO hybrids, the fabrication of the amorphous SiO₂ was confirmed from the XRD results as shown in the **Figure 18**. XRD peak of the pure SiO₂ confirmed the presence of amorphous SiO₂ in the sample, which is prepared from the same method and under same experimental conditions but without the addition of GO.

In the XRD spectra of all the samples with % rGO of 1.55, 6.75 and 10.82 and pure SiO₂, the presence of characteristic peaks of amorphous SiO₂ is evident and matched with JCPDS card no. 01-086-1561. Relatively intense and broader peaks are observed in the XRD of pure SiO₂, SiO₂-rGO-1.55% and SiO₂-rGO-6.75% hybrids in comparison to SiO₂-rGO-10.82% hybrid. In XRD pattern (**Figure 18**), the absence of XRD peak at 10.28° is the evidence of the successful reduction of GO in hybrids after hydrothermal and calcination treatments. Raman spectroscopy confirmed the presence of carbon in hybrids. Meanwhile, SiO₂-rGO hybrids were tested for FTIR spectra to evaluate the reduction of GO and successful attachments of SiO₂ spheres with rGO platelets, as shown in **Figure 19**. With 1.55, 6.75 and 10.82 wt.% rGO, it is found that SiO₂-rGO hybrids have shown IR band at 3417 and 1396 cm⁻¹, which are mainly due to the stretching and bending vibrations of —OH structural group and stretching vibrations of absorbed water.

All hybrids have shown the IR band at 1642 cm⁻¹, which is due to the bending vibration of absorbed water molecules. In SiO₂-rGO hybrids, the IR bands at 1110, 800 and 479 cm⁻¹ are assigned to the Si-O-Si asymmetric stretching and bending vibrations, respectively. According to previous reports, the IR bands at 1110, 800 and 479 cm⁻¹ are main IR characteristics bands for amorphous nature of silica, and such bands appear in IR spectra of all three SiO₂-rGO hybrids. In hybrids, IR band at 380 cm⁻¹ is associated with the Si-OH wagging mode. In-between 500 and 780 cm⁻¹, the appearance of IR bands is mainly because of assembling of SiO₂ spheres and rGO platelets in hybrids. Below 1000 cm⁻¹, IR bands are mainly due

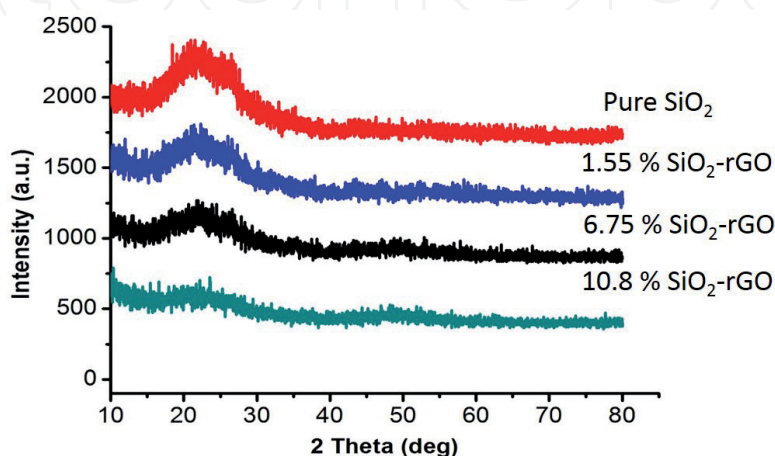


Figure 18. XRD of SiO₂-rGO hybrids with 1.55, 6.75 and 10.8% rGO and pure SiO₂ fabricated at a calcination temperature of 800 K for 1 h.

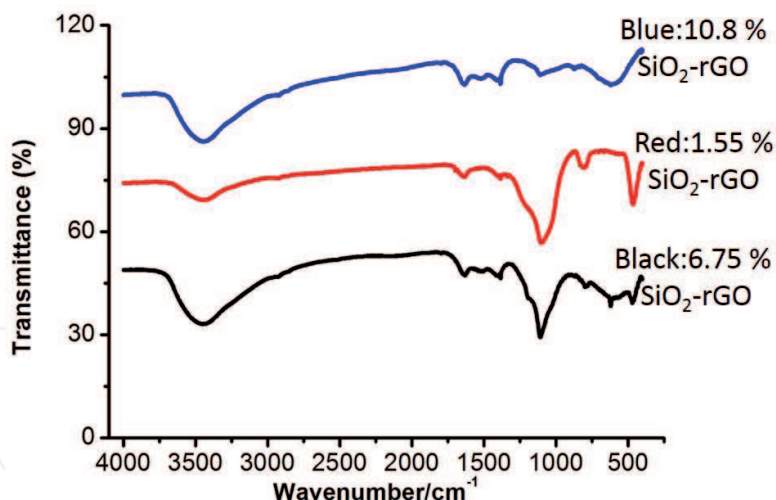


Figure 19.
FTIR of SiO_2 -rGO hybrids with 1.55, 6.75 and 10.8% rGO.

to reduced oxygen and —OH groups, which is a further indication of a successful reduction of GO in hybrids after hydrothermal and calcination treatments. FTIR spectra of all hybrids possess less pronounced IR bands, and which are associated with the presence of amorphous silica. Amorphous silica can be distinguished from crystalline silica based on far FTIR region measurements. For more information of the chemical composition and elemental states, the XPS spectroscopy of hybrids is carried out. With 1.55, 6.75 and 10.82 wt.% rGO, XPS spectra of SiO_2 -rGO hybrids is presented in **Figure 20**.

In case of all the hybrids, XPS spectra show distinct peaks for C1s, O1s, O2s, Si2s, and Si2p. In case of SiO_2 -rGO-10.82% hybrid, the intensity ratios of the C1s peak to the Si 2s and Si 2p peaks are measured, and intensity ratios are higher in comparison to hybrids with 6.75 and 1.55% rGO. This may be due to more rGO in hybrids, as confirmed by the TGA results. The samples were tested for Brunauer-Emmett-Teller (BET) surface areas. In hybrids, higher % of rGO helps to increase surface area compared to that of pure SiO_2 . With 1.55, 6.75 and 10.82% rGO, the nanohybrids of SiO_2 -rGO have BET surface areas of 611.21 ± 19.02 , 677.53 ± 25.21 , and $712.01 \pm 13.21 \text{ m}^2 \cdot \text{g}^{-1}$, respectively. For pure SiO_2 , the BET surface area is $333.07 \pm 21.57 \text{ m}^2 \cdot \text{g}^{-1}$. With 1.55, 6.75 and 10.82% rGO, the bulk densities of SiO_2 -rGO have values of 1.41 ± 0.07 , 1.29 ± 0.19 , and $0.89 \pm 0.03 \text{ g cm}^{-3}$, respectively. For bare SiO_2 , the bulk density is $2.75 \pm 0.12 \text{ g cm}^{-3}$. It is found that mesoporosity

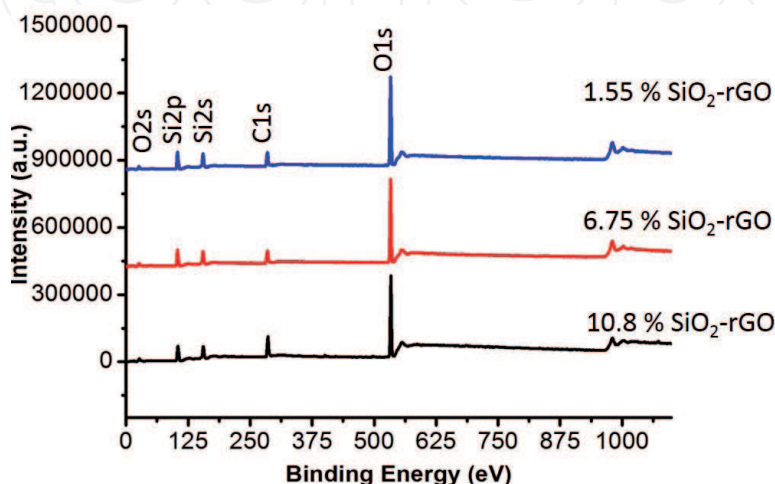


Figure 20.
XPS spectra of SiO_2 -rGO hybrids with 1.55, 6.75 and 10.8% rGO.

is highest with mesopores volume % of 90.52, which is measured for pure SiO₂. It is quite clear that minimum mesopores volume % is 57.11, which is calculated for SiO₂-rGO hybrid with 10.82% rGO. With higher wt.% of SiO₂, hybrids have shown an increase of mesopores volume %. Clearly, the presence of more rGO has led to higher BET surface area in hybrids. Well-aligned SiO₂ spheres with ultrathin rGO platelets resulted in a higher surface area and lower density compared to pure SiO₂. In hybrids, the presence of more rGO has increased the BET surface area, which is the main reason for enhanced thermal and electrical conductivity due to the availability of more surface electrons of rGO platelets. The higher value of surface areas, electrical conductivity and thermal conductivity are significant factors for applications in thermal and electrical engineering. The effect of hot pressing pressure on SiO₂ and rGO hybrid was conducted. Raman spectroscopy is conducted on SiO₂-rGO-6.75, which are hot pressed at 10, 20 and 30 MPa, respectively. The higher hot pressing pressure led the D peak intensity to reduce. For SiO₂-rGO-6.75 hybrid at 30 MPa, D peak is almost disappeared as compared to the hot-pressing pressure of 10 and 20 MPa. It shows that higher hot pressing pressure leads to remove defects from the rGO platelets and reconstruction of sp² carbon network in hybrid. The D/G intensity ratio has reduced with higher hot pressing pressure. Solvothermal-hot press processed SiO₂ and rGO hybrids have shown a significant improvement in the physical properties such as the electrical conductivity, thermal conductivity, tensile strength and the dielectric constant. In SiO₂-rGO-10.8% hybrid, the electrical conductivity of 0.143 S•m⁻¹ is calculated. For the same sample, the thermal conductivity of 1.612 Wm⁻¹ K⁻¹ is calculated, which is enhanced by more than 255%. With little rGO in hybrid, dielectric constant increases by seven orders of magnitude through second percolation threshold, such values for dielectric constants are higher. In solvothermal-hot press processed SiO₂-rGO, improved physical properties are due to more rGO platelets, high-temperature calcination, high-temperature hot pressing and formation of conductive pathways between rGO platelets and SiO₂ spheres.

5. Conclusions

This book chapter has explained ceramics-graphene hybrids, enhanced properties and possible applications in ceramics-graphene industry. Further, by the solvothermal-hot pressing method, a complete systematic study on enhanced physical properties of the hybrids has been made, which can further implement hybrids in advanced technological applications. This can lead to a significant contribution for the applications of ceramics-graphene assembly nanomaterials which can be further applied as electrolytes, catalysts, conductive, electrochemically active, and as dielectric materials for the high-temperature applications due to enhanced physical properties.

Conflict of interest

Authors have declared no “conflict of interest.”

IntechOpen

Author details

Mujtaba Ikram^{1*} and Muhammad Umer Farooq²

1 Department of Physics, Government College University (GCU), Lahore, Pakistan

2 Department of Physics, University of Education, Faisalabad Campus, Faisalabad, Pakistan

*Address all correspondence to: dr.muftabaikram@gcu.edu.pk

IntechOpen

© 2019 The Author(s). Licensee IntechOpen. This chapter is distributed under the terms of the Creative Commons Attribution License (<http://creativecommons.org/licenses/by/3.0>), which permits unrestricted use, distribution, and reproduction in any medium, provided the original work is properly cited. 

References

- [1] Sau TK, Rogach AL, Jäckel F, Klar TA, Feldmann J. Properties and applications of colloidal nonspherical noble metal nanoparticles. *Advanced Materials*. 2010;**22**:1805-1825. DOI: 10.1002/adma.200902557
- [2] Xia Y, Xiong Y, Lim B, Skrabalak SE. Shape-controlled synthesis of metal nanocrystals: simple chemistry meets complex physics. *Angewandte Chemie International Edition*. 2009;**48**:60-103. DOI: 10.1002/anie.200802248
- [3] Liu ZB, Xu YF, Zhang XY, Zhang XL, Chen YS, Tian JG. Porphyrin and fullerene covalently functionalized graphene hybrid materials with large nonlinear optical properties. *The Journal of Physical Chemistry B*. 2009;**113**:9681-9686. DOI: 10.1021/jp9004357
- [4] Sau TK, Rogach AL. Nonspherical noble metal nanoparticles: colloid-chemical synthesis and morphology control. *Advanced Materials*. 2010;**22**:1781-1804. DOI: 10.1002/adma.200901271
- [5] Markandan K, Chin JK, Tan MT. Recent progress in graphene based ceramic composites: a review. *Journal of Materials Research*. 2017;**32**:84-106. DOI: 10.1557/jmr.2016.390
- [6] Neto AC, Guinea F, Peres NM, Novoselov KS, Geim AK. The electronic properties of graphene. *Reviews of Modern Physics*. 2009;**81**:109. DOI: 10.1103/RevModPhys.81.109
- [7] Kim KS, Zhao Y, Jang H, Lee SY, Kim JM, Kim KS, et al. Large-scale pattern growth of graphene films for stretchable transparent electrodes. *Nature*. 2009;**457**:706-710. DOI: 10.1038/nature07719
- [8] Novoselov KS, Fal V, Colombo L, Gellert P, Schwab M, Kim K. A roadmap for graphene. *Nature*. 2012;**490**:192-200. DOI: 10.1038/nature11458
- [9] Novoselov KS, Geim AK, Morozov SV, Jiang D, Zhang Y, Dubonos SV, et al. Electric field effect in atomically thin carbon films. *Science*. 2004;**306**:666-669. DOI: 10.1126/science.1102896
- [10] Benavente R, Pruna A, Borrell A, Salvador M, Pullini D, Peñaranda-Foix F, et al. Fast route to obtain Al₂O₃-based nanocomposites employing graphene oxide: synthesis and sintering. *Materials Research Bulletin*. 2015;**64**:245-251. DOI: 10.1016/j.materresbull.2014.12.075
- [11] Bhowmik K, Chakravarty A, Bysakh S, De G. γ -Alumina nanorod/reduced graphene oxide as support for poly(ethylenimine) to capture carbon dioxide from flue gas. *Energy Technology*. 2016;**4**:1409-1419. DOI: 10.1002/ente.201600186
- [12] Chen L, Chai S, Liu K, Ning N, Gao J, Liu Q, et al. Enhanced epoxy/silica composites mechanical properties by introducing graphene oxide to the interface. *ACS Applied Materials & Interfaces*. 2012;**4**:4398-4404. DOI: 10.1021/am3010576
- [13] Huang D, Yang Z, Li X, Zhang L, Hu J, Su Y, et al. Three-dimensional conductive networks based on stacked SiO₂@graphene frameworks for enhanced gas sensing. *Nanoscale*. 2017;**9**:109-118. DOI: 10.1039/C6NR06465E
- [14] Kumar KS, Sanyadanam S, Paik P. Dangling ultrafine nano silica on graphene oxide to form hybrid nanocomposite: enhancement of dielectric properties. *Materials Research Express*. 2016;**3**:055019. DOI: 10.1088/2053-1591/3/5/055019
- [15] Lv L, Huang L, Zhu P, Li G, Zhao T, Long J, et al. SiO₂ particle-supported

- ultrathin graphene hybrids/
polyvinylidene fluoride composites
with excellent dielectric performance
and energy storage density. *Journal
of Materials Science: Materials in
Electronics*. 2017;**28**:13521-13531. DOI:
10.1007/s10854-017-7191-0
- [16] Watcharotone S, Dikin DA,
Stankovich S, Piner R, Jung I, Dommett
GH, et al. Graphene-silica composite
thin films as transparent conductors.
nano letters. 2007;**7**:1888-1892. DOI:
10.1021/nl070477
- [17] Qian R, Yu J, Wu C, Zhai X, Jiang P.
Alumina-coated graphene sheet
hybrids for electrically insulating
polymer composites with high thermal
conductivity. *RSC Advances*. 2013;**3**:
17373-17379. DOI: 10.1039/c3ra42104j
- [18] Walker LS, Marotto VR, Rafiee MA,
Korathkar N, Corral EL. Toughening
in graphene ceramic composites. *ACS
Nano*. 2011;**5**:3182-3190. DOI: 10.1021/
nn200319d
- [19] Akhtar F, Rehman Y, Bergström L.
A study of the sintering of
diatomaceous earth to produce porous
ceramic monoliths with bimodal
porosity and high strength. *Powder
Technology*. 2010;**201**:253-257. DOI:
10.1016/j.powtec.2010.04.004
- [20] Bhowmik K, Pramanik S, Medda
SK, De G. Covalently functionalized
reduced graphene oxide by organically
modified silica: a facile synthesis of
electrically conducting black coatings
on glass. *Journal of Materials Chemistry*.
2012;**22**:24690-24697. DOI: 10.1039/
c2jm35429b
- [21] Dervin S, Lang Y, Perova T,
Hinder SH, Pillai SC. Graphene oxide
reinforced high surface area silica
aerogels. *Journal of Non-Crystalline
Solids*. 2017;**465**:31-38. DOI: 10.1016/j.
jnoncrsol.2017.03.030
- [22] Porwal H, Grasso S, Reece M.
Review of graphene-ceramic matrix
composites. *Advances in Applied
Ceramics*. 2013;**112**:443-454. DOI: 10.11
79/174367613X13764308970581
- [23] Lwin S, Li Y, Frenkel AI, Wachs IE.
Nature of WO_x sites on SiO₂ and their
molecular structure-reactivity/selectivity
relationships for propylene metathesis.
ACS Catalysis. 2016;**6**:3061-3071. DOI:
10.1021/acscatal.6b00389
- [24] Merle N, Le-Quémener FDR,
Bouhoute Y, Szeto KC, De-Mallmann A,
Barman S, et al. Well-defined
molybdenum oxo alkyl complex
supported on silica by surface
organometallic chemistry: a highly
active olefin metathesis precatalyst.
*Journal of the American Chemical
Society*. 2017;**139**:2144-2147. DOI:
10.1021/jacs.6b11220
- [25] Ciriminna R, Fidalgo A, Pandarus V,
Béland F, Ilharco LM, Pagliaro M. The
sol-gel route to advanced silica-based
materials and recent applications.
Chemical Reviews. 2013;**113**:6592-6620.
DOI: 10.1021/cr300399c
- [26] Huang L, Zhu P, Li G, Lu DD, Sun
R, Wong C. Core-shell SiO₂@RGO
hybrids for epoxy composites with low
percolation threshold and enhanced
thermo-mechanical properties. *Journal
of Materials Chemistry A*. 2014;**2**:18246-
18255. DOI: 10.1039/C4TA03702B
- [27] Ramezanzadeh B, Haeri Z,
Ramezanzadeh M. A facile route
of making silica nanoparticles-
covered graphene oxide nanohybrids
(SiO₂-GO); fabrication of SiO₂-GO/
epoxy composite coating with superior
barrier and corrosion protection
performance. *Chemical Engineering
Journal*. 2016;**303**:511-528. DOI:
10.1016/j.cej.2016.06.028
- [28] Huang D, Li X, Wang S, He G,
Jiang W, Hu J, et al. Three-dimensional
chemically reduced graphene oxide
templated by silica spheres for ammonia
sensing. *Sensors and Actuators B*:

Chemical. 2017;252:956-964. DOI:
10.1016/j.snb.2017.05.117

[29] Zhibin L, Xue-Feng Y, Zhu P-K.
Recent advances in cell-mediated
nanomaterial delivery systems for
photothermal therapy. *Journal of
Materials Chemistry B*. 2018;6:1296-
1311. DOI: 10.1039/C7TB03166A

[30] Islam A, Mukherjee B, Sribalaji M,
Rahman OA, Arunkumar P, Babu KS,
et al. Role of hybrid reinforcement
of carbon nanotubes and graphene
nanoplatelets on the electrical
conductivity of plasma sprayed alumina
coating. *Ceramics International*.
2017;44:4508-4511. DOI: 10.1016/j.
ceramint.2017.12.021

IntechOpen